Available online at www.sciencedirect.com
ScienceDirect
C. R. Physique 8 (2007) 365–373
COMPTES RENDUS PHYSIQUE
http://france.elsevier.com/direct/COMREN/

Optical techniques for direct imaging of exoplanets/Techniques optiques pour l'imagerie directe des exoplanètes

Adaptive optics for direct detection of extrasolar planets: the Gemini Planet Imager

Bruce Macintosh [a,b,*], James Graham [a,c], David Palmer [a,b], Rene Doyon [d], Don Gavel [a,e], James Larkin [a,f], Ben Oppenheimer [a,g], Leslie Saddlemyer [h], J. Kent Wallace [a,i], Brian Bauman [a,b], Darren Erikson [h], Lisa Poyneer [a,b], Anand Sivaramakrishnan [a,g], Rémi Soummer [a,g], Jean-Pierre Veran [h]

[a] *NSF Center for Adaptive Optics, University of California, Santa Cruz, CA 95064, USA*
[b] *Lawrence Livermore National Laboratory, 7000 East Ave., Livermore, CA 94551, USA*
[c] *Department of Astronomy, University of California at Berkeley, Berkeley, CA 94720, USA*
[d] *Université de Montreal, Department de Physique, Montreal, QC, H3C 3J7, Canada*
[e] *UC Santa Cruz, 1156 High Street, Santa Cruz, CA 95064, USA*
[f] *Department of Physics and Astronomy, UC Los Angeles, Los Angeles, CA 90095, USA*
[g] *Department of Astrophysics, American Museum of Natural History, New York, NY 10024, USA*
[h] *Herzberg Institute of Astrophysics, 5071 West Saanich Road, Victoria, BC V8X 4M6, Canada*
[i] *Jet Propulsion Laboratory, California Institute of Technology, Pasadena, CA 91109, USA*

Available online 8 June 2007

Abstract

The direct detection of photons emitted or reflected by extrasolar planets, spatially resolved from their parent star, is a major frontier in the study of other solar systems. Direct detection will provide statistical information on planets in 5–50 AU orbits, inaccessible to current Doppler searches, and allow spectral characterization of radius, temperature, surface gravity, and perhaps composition. Achieving this will require new, dedicated, high-contrast instruments. One such system under construction is the Gemini Planet Imager (GPI). This combines a high-order/high-speed adaptive optics system to control wavefront errors from the Earth's atmosphere, an advanced coronagraph to block diffraction, ultrasmooth optics, a precision infrared interferometer to measure and correct systematic errors, and a integral field spectrograph/polarimeter to image and characterize target planetary systems. We predict that GPI will be able to detect planets with brightness less than 10^{-7} of their parent star, sufficient to observe warm self-luminous planets around a large population of targets. ***To cite this article: B. Macintosh et al., C. R. Physique 8 (2007).***

Résumé

Optique adaptative pour la détection directe d'exoplanètes : l'imageur d'exoplanètes de Gemini. La détection directe des photons émis ou réfléchis par des exoplanètes résolues angulairement de leur étoile est un pas décisif pour l'étude de nouveaux systèmes planétaires. La détection directe fournira des informations statistiques sur les planètes ayant une distance orbitale comprise entre 5 à 50 UA, ce qui est un intervalle de séparations qui demeure inexploré par les recherches actuelles basées sur l'effet Doppler, et permettra leur caractérisation : rayon, température, gravité de surface, et peut-être même la détermination de leur composition chimique. De nouveaux instruments sont nécessaires pour effectuer ces observations à fort contraste. Le planétographe

* Corresponding author.
E-mail address: bmac@igpp.llnl.gov (B. Macintosh).

1631-0705/$ – see front matter
doi:10.1016/j.crhy.2007.04.007

Gemini Planet Imager (GPI) est l'un de ces systèmes en construction. Il combine un système d'optique adaptative opérant à grande vitesse et comportant un important nombre d'actuateurs afin de corriger précisément les effets de la turbulence atmosphérique, un coronographe pour réduire la diffraction, des optiques très précises, un interféromètre infrarouge pour mesurer et corriger les erreurs systématiques et un spectrographe/polarimètre à champ intégral pour imager et caractériser les systèmes planétaires. Nous prévoyons que GPI détectera des exoplanètes dont le contraste par rapport à leur étoile est supérieur à 10^7, ce qui sera suffisant pour observer des planètes chaudes et lumineuses autour d'un grand nombre d'étoiles. ***Pour citer cet article : B. Macintosh et al., C. R. Physique 8 (2007).***

1. Introduction

More than 200 extrasolar planets have been detected using Doppler and transit techniques [1], leading to a revolution in our understanding of planetary systems. However, this revolution is still incomplete: several competing theories of planet formation and migration exist based on the observations of planets in unexpected regions. In the future, other techniques will begin to complement Doppler and transit, e.g., precision astrometry for measurement of planet masses [2]. The ability to directly detect extrasolar planets via emitted or reflected photons spatially resolved from its parent star will be a powerful complement to these techniques, allowing us to detect planets in orbits (5–50 AU) with periods too long for Doppler searches. Spectral characterization of directly-detected extrasolar planets would allow measurements of their radius, temperature, and surface gravity. At present, this is impractical: cameras and coronagraphs used with current AO systems are limited to contrast (defined as the ratio of observed planet brightness to observed parent-star brightness) of 10^{-5}–10^{-6} at large (>1 arcsecond) angles. This can allow detection of young (<10 Myr) planets [3] in exotic circumstances, but since young stars are distant these will necessarily only be visible in wide (>50 AU) orbits, often around very low mass primaries, and hence represent systems different from our own.

Contrasts of 10^{-7}–10^{-8}, though insufficient to detect a mature equivalent to Jupiter, can detect more massive planets through their self-luminosity to ages of 1 Gyr or more. Achieving such a contrast will require a new type of astronomical system, dedicated specifically to high-contrast imaging rather than being optimized for general use. The Gemini Planet Imager (GPI), currently under construction for the 8-m Gemini South telescope, is such an instrument. GPI has four major components. The primary AO system sharply attenuates atmospheric wavefront errors, optimized not for maximum Strehl but for best performance in the 'dark hole' region and minimal systematic errors. Diffraction is suppressed through an apodized-pupil Lyot coronagraph (APLC) which combines a conventional Lyot-type design with mild pupil apodization to shape the intensity in the Lyot plane. Tightly integrated with the coronagraph is an infrared interferometric wavefront sensor. This serves as a calibration system, measuring the time-averaged wavefront during a science exposure. This information can be used to modify the main AO system control point to remove residual static errors. Finally, the science light is fed into a near-IR Integral Field Spectrograph (IFS).

Images produced by such systems have a different morphology than classical AO images. If the deformable mirror (DM) has regularly-spaced actuators that project to a separation d on the primary mirror, it can control wavefront errors up to a spatial frequency of $1/2d$. This results in a residual wavefront error power spectrum that sharply drops off within the so-called 'control radius' (really a square) of frequencies lower than this cutoff. By Fourier optics [4], this highest controlled frequency will correspond to a angular separation in the point spread function (PSF) $\lambda/2d$. The result is an image in which most light within a square 'dark hole' region λ/d on each side has been removed (Fig. 1).

For a AO system correcting a dynamically-moving atmosphere, the correction is imperfect, of course; some scattered light will remain due to the delay between measuring and correcting the wavefront and noise in that measurement purpose. Classical AO systems do not produce such a dark hole both due to relatively large wavefront errors and due to aliasing of (uncorrectable) high-frequency errors in the wavefront sensor. For a high Strehl ratio AO system, this aliasing can be prevented by spatially-filtering the light going to the wavefront sensor [5] with a filter of size λ_{wfs}/d.

Table 1 lists the key properties of the GPI system and Fig. 2 shows a schematic overview. Fig. 3 shows a CAD rendering of the instrument design. Light enters at the top right and is relayed between the two deformable mirrors. Visible light (<0.95 microns) is split off to the spatially-filtered Shack–Hartmann wavefront sensor. The IR light passes through a pupil plane at which we place input pupil masks such as apodizers. It then continues to converge to focus. At this plane we place reflective occulting masks; the core of the PSF passes through a hole in the occulting

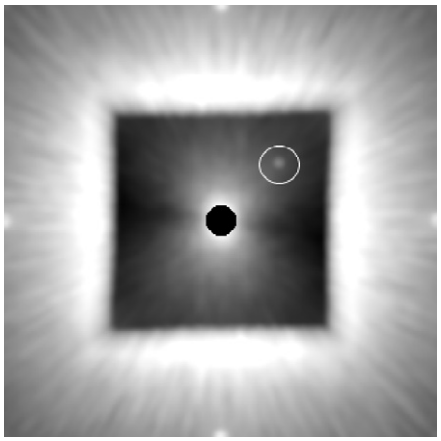

Fig. 1. Simulated GPI image. This 20-second exposure of a solar-type star at 10 pc was generated using a Fraunhoffer-optics Monte Carlo simulation of the AO system and an idealized apodized coronagraph. A 200 Myr/5 Jupiter mass planet at 6 AU separation is circled.

Table 1
Key system parameters

AO subsystem	
Primary deformable mirror	4096-actuator Boston Micromachines MEMS
Subaperture size	$d = 18$ cm ($N = 44$ subapertures across primary mirror)
Wave front sensor type	Spatially-Filtered Shack–Hartmann Wave Front Sensor (SFWFS)
Wave front sensor CCD	128×128 pixels (goal: 180×180)
Maximum frame rate	2000 Hz
Reconstructor	Optimal Fourier Transform Reconstructor
Limiting magnitude	$I < 8$ mag. (goal: $I < 9$ mag.)
Typical Strehl ratio @ 1.6 microns	0.9 ($I = 7$ mag., $r_0 = 14.5$ cm)
Optics	
Surface quality	<5 nm RMS WFE per optic
Coronagraph subsystem	
Type	Apodized-Pupil Lyot Coronagraph (APLC)
Inner working distance	$\sim 3\lambda/D$
Transmission	>60%
Calibration subsystem	
Type	Infrared interferometric wave front sensor
Wavelength range	1–2.4 μm
Wave front measurement precision	1 nm RMS in controlled frequency range
Science Instrument	
Type	Lenslet-based integral field spectrograph
Lenslet size	0.014×0.014 arcseconds
Field of view	2.8×2.8 arcseconds
Spectral resolution (2-pixel)	$\Delta\lambda/\lambda \sim 45$
Spectral coverage	One of Y, J, H or K band per exposure (20% bandwidth)
Detector	HAWAII-II RG

mask and into the calibration system while the outer part of the PSF is reflected. The resulting beam is collimated and split between the calibration system and the science integral field unit. The beam enters the IFU collimated, with the (selectable) cryogenic Lyot stop pupil located just inside the dewar.

2. The AO system

The primary purpose of the adaptive optics system is to sense and correct wavefront phase aberrations. The wavefront sensor is a visible-light (0.7–0.9 μm) spatially-filtered Shack–Hartmann wavefront sensor (SFWFS). The square spatial filter is matched to the subaperture sampling λ/d and prevents aliasing of dynamic and static wavefront errors.

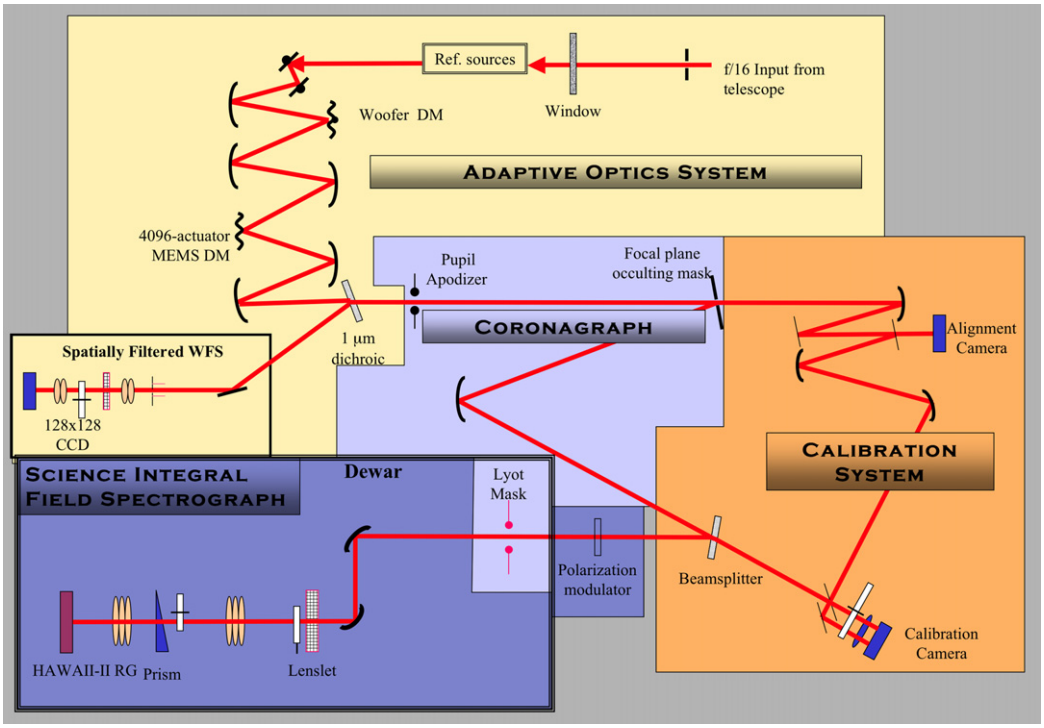

Fig. 2. Schematic layout of the Gemini Planet Imager.

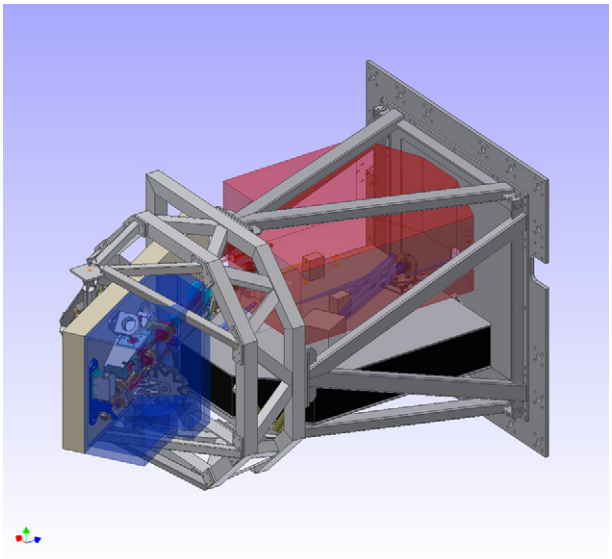

Fig. 3. CAD rendering of the GPI design. The square face on the right, 1.2 meters on a side, mounts to the Gemini Cassegrain Instrument Support Structure. The AO components are located on the lower optical bench, the IR calibration WFS on the diagonal bench at the rear, and the integral field spectrograph in the red dewar above the AO bench. (For interpretation of the references to colour in this figure legend, the reader is referred to the web version of this article.)

Since AO servo lag is a major source of scattered light within the dark hole, it is important for the system to operate as fast as possible, with a goal of a total system update rate of 2.5 kHz and AO corrections applied in <1 frame time of delay. The baseline CCD is a conventional 128×128 pixel device manufactured by Lincoln Laboratories (although we are studying other CCD technologies); for the GPI geometry (44 subapertures in the pupil diameter) this leads to

operation in a 2×2 pixel 'quad-cell' mode. Quad-cell centroiding of unresolved Shack–Hartmann spots can lead to uncertainties in the absolute gain of the sensor—the scaling between wavefront slope and centroider output—as fluctuations in the atmospheric turbulence strength r_0 cause the size of the spots to vary. However, the SFWFS removes high-frequency aberrations within each subaperture, causing the GPI gain to vary by less than 1% as r_0 varies from 10 to 30 cm.

The Shack–Hartmann sensor measures wavefront slopes in each subaperture location, which are then reconstructed into a wavefront using an adaptive algorithm called Optimal Fourier Control (OFC) [6]. At each time step, the slope measurements obtained from the spatially filtered Shack–Hartmann WFS are reconstructed into a residual phase estimate using the computationally efficient Fourier Transform Reconstruction (FTR) method. This method reconstructs the phase in Fourier modes—a convenient modal set for ExAO, since each Fourier mode scatters light to a specific spatial location in the PSF. Telemetry of the closed-loop modal coefficients is saved, and then used in a supervisory process to estimate the temporal PSDs of the atmosphere and the noise. The optimal control loop gain for each independent Fourier mode is calculated and used to provide wavefront control which minimizes the PSF intensity by location in the controllable region. Using this algorithm, the computational load is ∼3 billion operations per second, within the reach of current general-purpose computers.

Commands from the wavefront sensor drive a Micro-electro-mechanical-system (MEMS) deformable mirror with $N = 44$ controlled actuators across the pupil. This deformable mirror is lithographically micromachined from silicon, with electrostatic actuators coupled to a gold-coated continuous mirror face. The resulting device is extremely compact—300–400 microns per actuator—which reduces the size of the entire system. Development of this DM is currently underway, based on the $N = 32$ Boston Micromachines mirror [7]. Actuator yield was a significant concern in the early Boston DMs, but recent laboratory testing has shown yields of ∼99.5% with no dead actuators in the central 90% inscribed circle of the mirror. The DM will be manufactured in a 64×64 format to increase the probability of finding a useable circular region.

The MEMS DM will have only 3–4 microns (surface) stroke, insufficient to fully correct the atmosphere on a 8-m telescope. We will therefore operate a woofer/tweeter architecture, offloading low-frequency modes from the MEMS to lower-order ($N = 8$) high-stroke conventional DM, referred to as a 'woofer'. The AO control software will allocate the wavefront correction between the two DMs on the basis of spatial frequency. The woofer mirror will also sever as the primary tip/tilt control, mounted on a fast steering platform.

3. Coronagraph

Light is scattered into the halo of the point spread function both by wavefront errors and by diffraction [4]—even a perfect telescope in space will have a bright Airy pattern that will prevent detection of planets. Controlling this diffraction is the role of a coronagraph. We carried out an extensive study of different options before selecting the Apodized Pupil Lyot Coronagraph (APLC) [8]. This combines a moderate apodization of the coronagraph input pupil (Fig. 4) with a classic Lyot architecture to strongly suppress diffraction at radii greater than $3\lambda/D$. Although the required level of apodization is only 90–95% at the edges of the pupil, manufacturing the apodizers remains a significant technical challenge. GPI will have selectable wheels to allow different combinations of apodizer, focal plane mask, and Lyot stop to be selected, e.g. for different observational wavelengths.

4. Precision infrared wavefront sensor

Fundamental limitations in the adaptive optics system—the finite supply of photons for wavefront sensing per timestep and the finite update rate of the system—will produce residual wavefront errors on the order of 80–100 nm RMS. This produces an image with a residual speckle pattern of contrast 10^{-5}, significantly brighter than target planets. However, these errors will be random; the residual image speckles they produce will fluctuate on a timescale comparable to the clearing time of the wind blowing across the telescope aperture [9], ultimately producing a smooth PSF halo in a long-exposure image. Planets at contrast levels of 10^{-7} can be detected against this smooth background.

If any systematic source of wavefront error is present, the halo will not become smooth. A small bias, e.g., due to optical aberrations present in the wavefront sensor but absent in the science-light path, will be invisible in a short-exposure image, but in a long-exposure image will produce quasi-static speckle patterns that completely swamp the signals of target planets. To achieve 10^{-7} contrast with GPI we require these errors remain below ∼1 nm over the

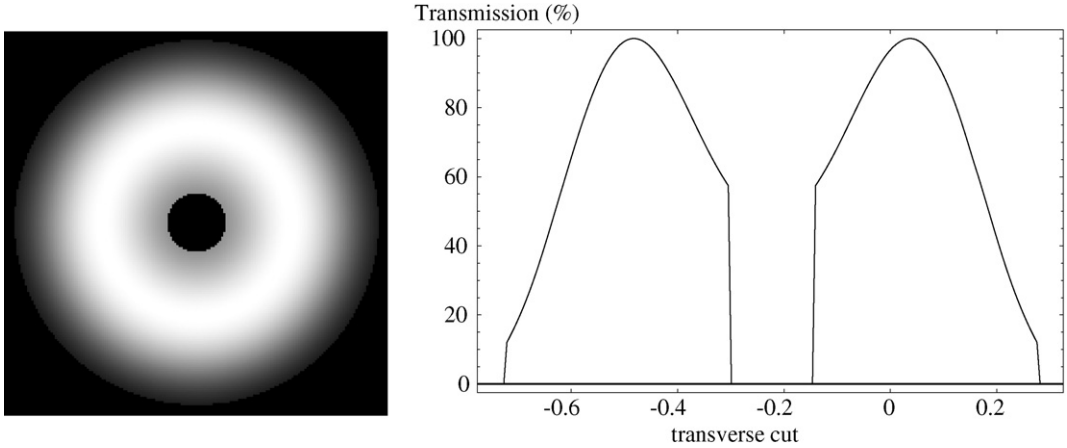

Fig. 4. Example of apodizer transmission for the Gemini Telescope geometry [8]. The minimum intensity transmission is 12% at the edges, and throughput is high: 63%. A classical Lyot coronagraph with an undersized Lyot stop has a typical throughput of 40% in contrast. The matched FPM has a diameter of $4.7\lambda/D$.

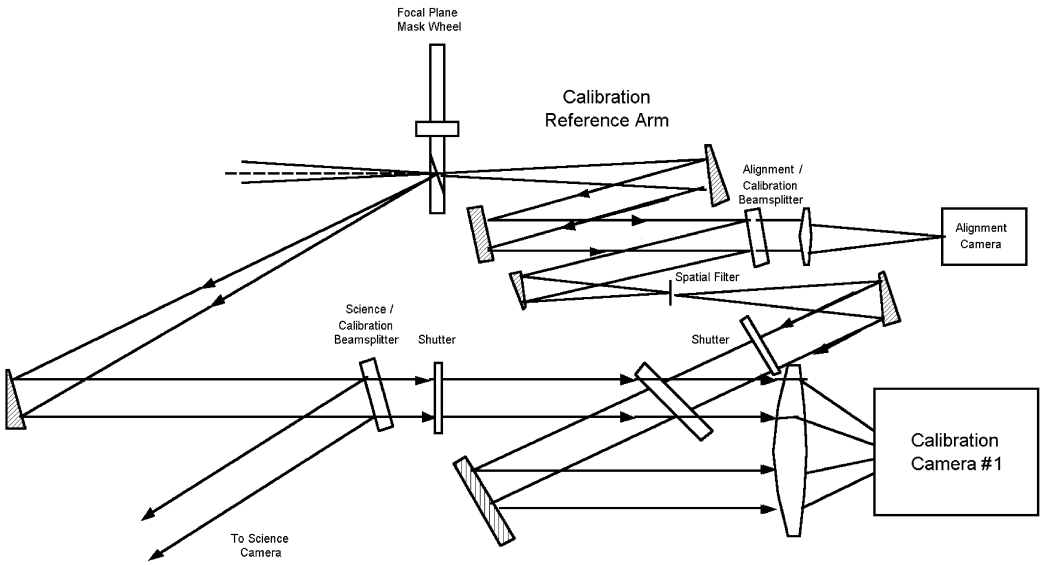

Fig. 5. A simple illustration of the calibration system. The science beam is on the left hand side of the image, while the reference arm and alignment and calibration camera are on the right. The path lengths are matched to within a few microns. The alignment camera insures the PSF is centered on the occulting mask. The calibration camera measures the wave front of the in the science beam.

controlled range of spatial frequencies—an extremely challenging goal. To achieve this, we will integrate a second high-precision IR wavefront sensor designed to measure the wavefront after the coronagraph focal plane.

The selected architecture is a modified Mach–Zehnder interferometer.

Fig. 5 shows a simple version of the calibration sensor. Light from the core of the PSF is removed at the coronagraph focal plane to provide a reference wavefront. Off-axis (science) light is sampled by a neutral beamsplitter and interfered with the reference light to provide wavefront measurements [10].

Locating the calibration system after the occultor simplifies its operation. By removing the coherent core of the starlight, the coronagraph focal-plane mask acts to convert phase errors into amplitude errors. As a result, the interferometer measurement does not require high accuracy in phase and any wavefront errors after the FPM will have little effect. This sensor will measure the wavefront at the science wavelength at $\sim$100 Hz and time-average it over 1–10 second intervals to remove atmospheric effects. Operating at the science wavelength it can sense all chromatic effects in the system; integrated with the coronagraph, the key location for the wavefront to be flattened, it has essen-

tially no non-common-path errors. (Wavefront errors after the coronagraph have only small effects on the PSF.) The reconstructed wavefront is then propagated forward to a set of offset commands for the primary AO system. Since the sensor can only see modes that come from the wings of the PSF, it is blind to tip/tilt and low-order modes. A separate pointing sensor/low-order wavefront sensor will track these modes.

5. Integral field spectrograph

The primary purposes of the GPI science instrument are to detect planetary companions by distinguishing them from PSF speckle noise, to record low-resolution 1–2.5 μm spectra of these planets, and to detect and measure circumstellar dust through polarization. The basic concept of multiwavelength speckle rejection has been described in several sources [11,12]. This technique, though potentially powerful, is extremely sensitive to differential chromatic aberrations; even a small amount of differential wavefront error can produce speckle patterns that vary strongly with wavelength [13]. To minimize this, we adopt a IFS design similar to the OSIRIS Keck instrument [14], using an array of lenslets to dissect the beam before the dispersing elements. Since it is extremely difficult to scatter light between different lenslet beams, aberrations in the dispersed beam—the most likely location for chromatic aberrations—are essentially irrelevant. The price of this architecture is paid in detector pixels; individual spectra must be well-separated on the detector (4–5 pixels between adjacent lenslet spectra). To achieve a reasonable field of view (2.8×2.8 arcseconds) the GPI IFS design has a spectral resolution of $\sim$45. Models show this is sufficient to measure effective temperature and surface gravity for typical planetary targets, since planets are dominated by broad molecular features. The IFS will also include a polarimetric mode used to characterize circumstellar dust.

6. Error budget and performance

Verifying the performance of a high-contrast AO system through the simulation is challenging. Many small static effects—e.g. uncalibrated non-common-path errors—only begin to significantly impact the PSF in multi-minute exposures, far too long for practical simulation. We therefore have taken a multilayered approach to simulation. Numerical simulations of the full AO system are used to evaluate performance of AO and coronagraph components in rejecting atmospheric wavefront errors and in evaluating performance as a function of star magnitude. Static optical effects are evaluated with stand-along simulations and their contrast effects added independently. Fig. 6 shows the predicted performance for both dynamic (atmosphere/AO) compared to the effect of 1 nm of residual static wavefront error. GPI simulations have been carried out using a range of r_0 values, based primarily on a typical $r_0 = 14.5$ cm atmosphere generated from Gemini and other site-monitoring campaigns (see for example [15]).

To evaluate the magnitude of different effects—including amplitude errors such as internal or external scintillation—we use a purely analytic error budget.

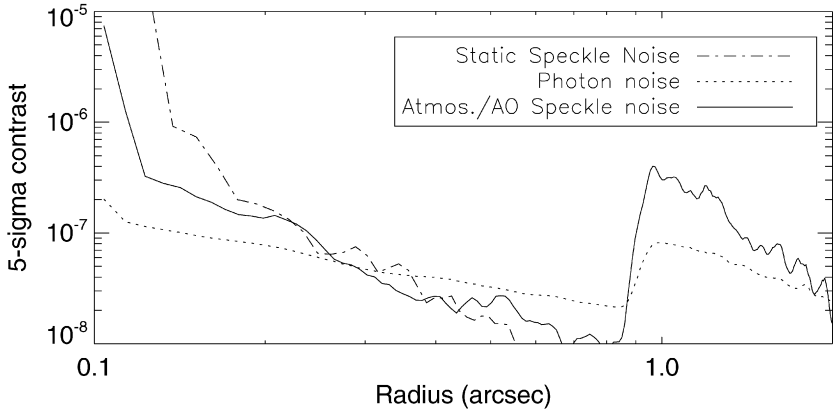

Fig. 6. Contrast versus radius from GPI simulations of a 1-hour H integration on a $I = 6$ mag. target star in a Cerro Pachaon $r_0 = 15$ cm atmosphere with 1 nm of additional static wavefront error. Curves show the residual noise due to photon statistics, atmosphere/AO speckles, and quasi-static speckles. No post-processing or speckle suppression is assumed.

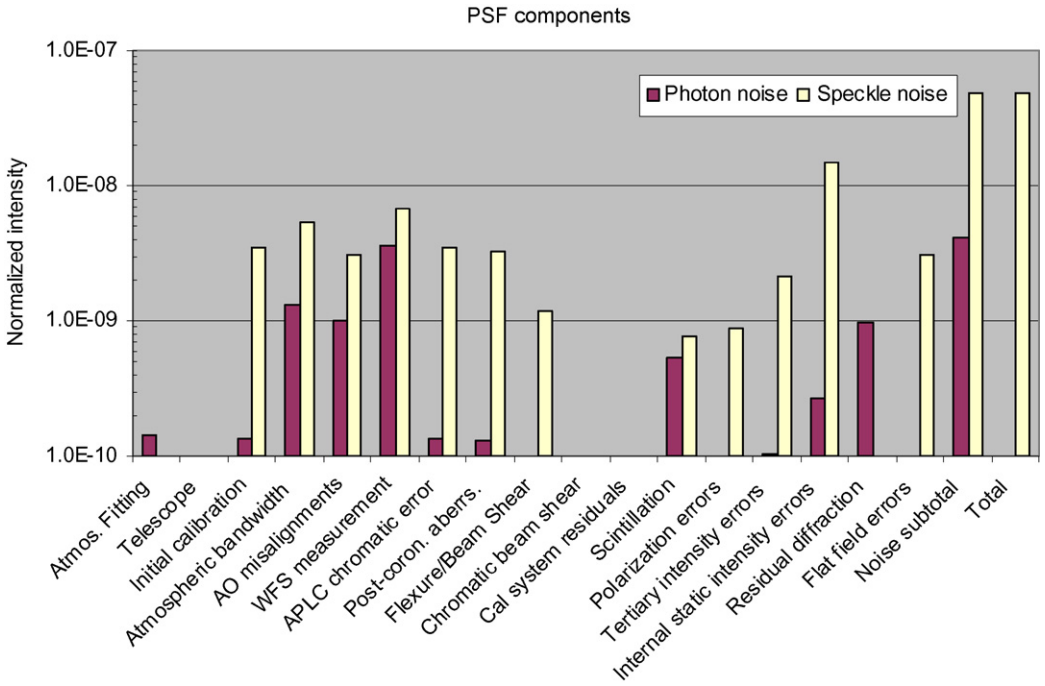

Fig. 7. Contrast error budget for a 1-hour observation of a $I = 5$ mag target, showing the speckle noise (which can be partially suppressed by multi-wavelength imaging) and Poisson photon noise for various error sources in the GPI system.

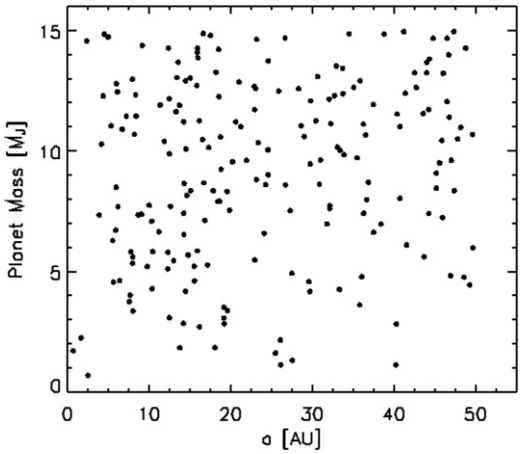

Fig. 8. The distribution of GPI-detected exoplanets in the semimajor axis/exoplanet mass plane. The detected planets are drawn from the field survey of nearby (<50 pc) stars (no age cut). This experiment samples semimajor axes and masses with uniformity.

Fig. 7 shows a realization of one such error budget. Dominant error sources are WFS measurement noise and internal static errors. In particular, internal phase-induced intensity errors from optics at non-pupil conjugates are potentially the largest source of quasi-static speckles—'internal scintillation'. These were evaluated through numerical wave-optics propagation. To reduce these to an acceptable level, each GPI optic will be manufactured to ∼5 nm RMS wavefront error, with some crucial surfaces manufactured to ∼3 nm RMS. The Gemini tertiary mirror induces similar errors; to avoid these, GPI may operate in an "up-looking" orientation that bypasses this tertiary optic. These effects are particularly troublesome in that they may produce speckle patterns whose radial scaling is more complex than pupil-plane errors and hence be more difficult to subtract with multiwavelength techniques [16]. Overall, the

guiding philosophy has been to use compact high-quality optics through the system to minimize common-path and non-common-path wavefront errors.

7. Conclusions

We are currently planning for first light in late 2010. When deployed, the Gemini Planet Imager—together with its European counterpart [17]—should be capable of achieving contrast 1–2 orders of magnitude better than current AO systems. This performance improvement—comparable to the gain from CCDs over photographic plates—is achieved not just through maximizing Strehl ratio but through careful minimization and control of static and quasi-static wavefront errors. GPI will be capable of observing a large sample of targets to $I = 8$ magnitude and imaging young or massive planets around targets in young associations and the solar neighborhood. Combining the numerical simulations discussed above with Monte Carlo models of the planet and star populations, we can predict the planet discovery rate for various assumptions.

Fig. 8 shows a representative outcome from one such simulation, in which the existing Doppler planet distribution is extrapolated from 5–50 AU at a rate of one giant planet per target star. A survey of 500 stars in the solar neighborhood selected to have age below 2 Gyr would discover $\sim$100 planets.

Acknowledgements

This research was performed under the auspices of the U.S. Department of Energy by the University of California, Lawrence Livermore National Laboratory under Contract W-7405-ENG-48, and also supported in part by the National Science Foundation Science and Technology Center for Adaptive Optics, managed by the University of California at Santa Cruz under cooperative agreement No. AST-9876783. We also acknowledge support from the Natural Science and Engineering Council of Canada. The Gemini Observatory is operated by the Association of Universities for Research in Astronomy, Inc., under a cooperative agreement with the NSF on behalf of the Gemini partnership: the National Science Foundation (United States), the Particle Physics and Astronomy Research Council (United Kingdom), the National Research Council (Canada), CONICYT (Chile), the Australian Research Council (Australia), CNPq (Brazil), and CONICET (Argentina).

References

[1] See for example http://exoplanet.eu/ for a current list.
[2] See M. Perryman, et al., Report by the ESA-ESO Working Group on Extra-Solar Planets, e-print astro-ph/0506163.
[3] G. Chauvin, et al., A giant planet candidate near a young brown dwarf. Direct VLT/NACO observations using IR wavefront sensing, Astron. Astrophys. 425 (2004) L29.
[4] M. Perrin, et al., The structure of high Strehl ratio point-spread functions, Astrophys. J. 596 (2003) 702.
[5] L. Poyneer, B. Macintosh, Spatially-filtered wave-front sensor for high-order adaptive optics, J. Opt. Soc. Amer. A 21 (2004) 810.
[6] L. Poyneer, J.-P. Veran, Optimal modal Fourier transform wavefront control, J. Opt. Soc. Amer. A 22 (2005) 1515.
[7] J. Evans, et al., Extreme adaptive optics testbed: performance and characterization of a 1024-actuator MEMS deformable mirror, Proc. SPIE 6113 (2006) 131.
[8] R. Soummer, Apodized pupil Lyot coronagraphs for arbitrary telescope apertures, Astrophys. J. 618 (2005) L161.
[9] B. Macintosh, et al., Speckle lifetimes in high-contrast adaptive optics, Proc. SPIE 5903 (2005) 170.
[10] J.K. Wallace, et al., Science camera calibration for extreme adaptive optics, Proc. SPIE 5490 (2004) 370.
[11] C. Marois, et al., Efficient speckle noise attenuation in faint companion imaging, Publ. Astron. Soc. Pacific 117 (2000) 91.
[12] W. Sparks, H. Ford, Imaging spectroscopy for extrasolar planet detection, Astrophys. J. 578 (2002) 543.
[13] C. Marois, et al., TRIDENT: An infrared differential imaging camera optimized for the detection of methanated substellar companions, Publ. Astron. Soc. Pacific 117 (2005) 745.
[14] J. Larkin, et al., OSIRIS: Integral field spectrograph for the Keck adaptive optics system, Proc. SPIE 4841 (2003) 1600.
[15] A. Tokovinin, T. Travouillon, Monthly Not. R. Astron. Soc. 365 (4) (2006) 1235–1242.
[16] C. Marois, D. Phillion, B. Macintosh, Exoplanet detection with simultaneous spectral differential imaging: effects of out-of-pupil-plane optical aberrations, Proc. SPIE 6269 (2006), in press.
[17] T. Fusco, et al., Design of the extreme AO system for the planet finder instrument on the VLT, Proc. SPIE 6272 (2006), in press.